



Contents lists available at ScienceDirect

Arabian Journal of Chemistry

journal homepage: www.ksu.edu.sa

Enhanced degradation of decabromodiphenyl ether (BDE-209) using ferrate (VI)-peroxymonosulfate combined process: Influencing factors, reaction kinetics, pathways, and toxicity control

Qi Han^{a,b}, Yi Huang^b, Peng Liu^c, Fan Zhang^b, Xiaodan Chen^b, Yurong Gu^{d,*}, Zijun Dong^{e,*}, Boping Yu^b, Linshen Xie^b

^a School of Civil and Environmental Engineering, Harbin Institute of Technology, Shenzhen, Shenzhen 518055, China

^b Shenzhen Academy of Environmental Sciences, Shenzhen 518001, China

^c School of Environmental and Civil Engineering, Dongguan University of Technology, Dongguan 523808, China

^d Shenzhen Polytechnic, Shenzhen 518055, China

^e School of Civil and Traffic Engineering, Shenzhen University, Shenzhen 518055, China

ARTICLE INFO

Keywords:

Ferrate(VI)
Peroxymonosulfate
Decabromodiphenyl ether
Degradation
Toxicity
Pathway

ABSTRACT

In this study, enhanced degradation of decabromodiphenyl ether (BDE-209) was systematically investigated using ferrate(VI)-peroxymonosulfate (Fe(VI)-PMS) combined process, including influencing factors (oxidant dosages (0.01–0.5 mmol/L), initial pH (3.0–11.0), temperatures (10–30 °C) and BDE-209 concentrations (0.5–5.0 μmol/L)), reaction kinetics, products (inorganic and organic ones), pathways and toxicity control. Compared to the sole Fe(VI) and PMS oxidation process, the Fe(VI)-PMS combined process exhibited a synergistic effect on BDE-209 degradation. Under pH 7.0 and 30 °C, complete degradation of BDE-209 (0.5 μmol/L) was achieved within 60 min by low dosages of Fe(VI) and PMS (0.1 mmol/L). Additionally, Fe(VI)-PMS combined process demonstrated strong adaptability to a wide pH range (5.0–9.0), maintaining over 85 % removal of BDE-209. Active species, including •OH and SO₄^{•-}, contributed to the oxidative removal of BDE-209. The detection of inorganic products indicated a 66.87 % debromination rate in Fe(VI)-PMS combined process, with no bromate by-products formed. Lower brominated intermediates were identified as the primary organic products, undergoing various reaction pathways such as debromination, radical addition, substitution, beta scission and oxidation. Moreover, toxicity assessment revealed effective control of the relative inhibitory rate of water samples (reduced to 3.56 %), significantly lower than that of BDE-209 itself (15.0 %). In practical water treatment applications, over 95 % removal of BDE-209 was achieved, highlighting the prospective potential of Fe(VI)-PMS combined process in organic pollutant degradation.

1. Introduction

As a class of brominated flame retardants, polybrominated diphenyl ethers (PBDEs) have been widely used in industrial products such as rubber, plastics, textiles, electronics, et al. (Yu et al., 2020). PBDEs are typically mixtures of 209 congeners. Among of them, decabromodiphenyl ether (deca-BDE, BDE-209) is the most prevalent one in commercial PBDEs family, accounting for over 80 % of annual PBDEs usage (Ji et al., 2017). Due to its extensive production and utilization, BDE-209 might release to the surrounding environment in the processes of production, application, disposal and recycling. Owing to its environmental persistence and bioaccumulate, BDE-209 has been frequently detected in water, air, soil,

sediment, aquatic organisms and even human tissues (Shi et al., 2015; Panda and Manickam, 2019; Cheng et al., 2021; Shao et al., 2021). Moreover, BDE-209 exhibits neurotoxicity, hepatotoxicity, endocrine toxicity, propagation toxicity and potential carcinogenicity (Wu et al., 2018; Wang et al., 2023; Han and Zheng, 2018), posing risks to both wildlife and human health. Studies have shown higher propagative toxicity of BDE-209 in *Daphnia magna* than that of growth, with a 48-hour median lethal concentration (LC₅₀) of 8.74 mg/L (Wang et al., 2023). And BDE-209 exposure has been linked to damage to barrier function and intestinal structure (Han and Zheng, 2018). Thus, there is a critical need to develop effective methods for BDE-209 degradation to mitigate its adverse effects on the environment and human health.

* Corresponding authors.

E-mail addresses: liupeng2@dgut.edu.cn (P. Liu), 651863124@qq.com (Y. Gu), dongzijun@szu.edu.cn (Z. Dong).

<https://doi.org/10.1016/j.arabjc.2024.105729>

Received 9 August 2023; Accepted 12 March 2024

Available online 14 March 2024

1878-5352/© 2024 The Authors. Published by Elsevier B.V. on behalf of King Saud University. This is an open access article under the CC BY-NC-ND license (<http://creativecommons.org/licenses/by-nc-nd/4.0/>).

Over the years, many approaches have been explored for BDE-209 removal, such as biological degradation, photochemical degradation, Fenton oxidation, and zero-valent iron reduction degradation (Qu et al., 2017; Guo et al., 2019; Tso and Shih, 2017; Sun et al., 2024; Ma et al., 2023). However, these methods often suffer from some inherent drawbacks such as long periods, high costs, substantial sludge generation, and operational challenges (as shown in Table 1). In addition, the debromination of BDE-209 using these techniques is often insufficient, as the more toxic lower-brominated intermediates are highly resistant to degrade (Yao et al., 2021). However, most researches have focused on the removal and toxicity of BDE-209 itself and individual intermediates, with limited information available on the comprehensive toxicity of the treated water samples during the degradation process (Table 2).

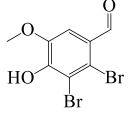
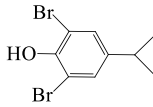
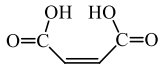
In recent years, ferrate(VI) (Fe(VI)) oxidation and sulfate radical ($\text{SO}_4^{\bullet-}$) based oxidation have confirmed as promising technologies for degrading refractory pollutants (Qu et al., 2020; Giannakis et al., 2021; Hou et al., 2021; Xiong et al., 2021; Su et al., 2022). Ferrate(VI) exhibits strong oxidative capabilities with redox potentials of 2.20 V in acidic and 0.72 V in alkaline conditions. Meanwhile, its final product Fe(III) is typical $\text{Fe}(\text{OH})_3$ colloid, which possess adsorptive properties for pollutant removal. Furthermore, ferrate(VI) oxidation could mitigate the formation of chlorinated and ozonated disinfection by-products (DBPs), enhancing its environmental friendliness. Thus, previous studies have demonstrated the efficacy of ferrate(VI) oxidation in eliminating refractory contaminants, owing to its multifaceted roles in oxidation, absorption, precipitation, coagulation and disinfection (Han et al., 2013; Han et al., 2015; Han et al., 2018; Han et al., 2019). However, given the relatively high cost of ferrate(VI) agent, some research efforts have focused on developing combined technologies for broader applications [18,20,24].

Advanced oxidation processes (AOPs) based on sulfate radical ($\text{SO}_4^{\bullet-}$) have also attracted increasing attentions because of their strong oxidation ability (with a high redox potential of 2.5 ~ 3.1 V and a long half-life of 30 ~ 40 μs), which could endow them high reactivity and long contacting time with organic pollutants, thereby improving removal efficiency (Oh et al., 2016; Lin et al., 2018). $\text{SO}_4^{\bullet-}$ can be generated by activating persulfate (PS, $\text{S}_2\text{O}_8^{2-}$, 2.01 V) or peroxymonosulfate (PMS, HSO_5^- , 1.82 V). It was reported that the unoccupied molecular orbital of PMS has a lower energy than that of PS, indicating that it is easier for PMS to accept electrons (Antoniou et al., 2010). In addition, PMS can be activated more easily owing to its asymmetric structure (Wu et al.,

Table 1
Results, advantages and disadvantages of BDE-209 degradation methods.

Degradation methods	Degradation rate	Advantages	Disadvantages	Reference
Biodegradation	30 %~90 %	low cost, in-situ remediation	long time, difficult control	(Yu et al., 2020; Wu et al., 2018)
Photochemical degradation	>95 %	low cost, fast, high efficiency, easy to implement	high toxic products generation	(Cheng et al., 2021; Wang et al., 2023)
Fenton oxidation	62 %~96 %	fast, controllable, easy to implement	high toxic products generation, large sludge production	(Panda and Manickam, 2019; Tso and Shih, 2017)
Zero-valent iron degradation	60 %~92 %	low cost and pollution	long time, difficult open-loop	(Han and Zheng, 2018; Qu et al., 2017; Qu et al., 2020)
Chemical oxidative degradation	>85 %	fast, high efficiency, easy to implement	high cost	(Shi et al., 2015; Guo et al., 2019)

Table 2
Mass spectra data of intermediate products by GC-MS/MS.

Products	Retention time (min)	Molecular weight (m/z)	Detected ions (m/z) (% abundance)	Molecular structure
A	16.60	959	799[100] 530 [21] 458 [37] 400 [87]	BDE-209
B	14.78	799	799[24] 641 [100] 482[14] 321 [46]	BDE-203, oct-BDE
C	11.06	563	563[49] 406 [1 0 0] 297[19] 202 [17]	BDE-99, hetpa-BDE
D	10.57	308	309[100] 312 [47]307[42] 267[14]	
E	9.16	294	294[100] 297 [55] 63[42] 131 [18]	
F	5.60	116	116 [27] 55 [1 0 0] 68 [43] 82 [40]	

2018). Fe(VI) has recently been demonstrated to be able to activate PMS to generate $\text{SO}_4^{\bullet-}$ (Gong et al., 2020). Therefore, the combination of Fe (VI) and PMS has been considered an innovative technology for the treatment of organic pollutants (Feng et al., 2017; Sun et al., 2018; Gong et al., 2020), which could overcome the limitations of these two oxidation methods (Feng et al., 2017). In addition, the combined use of Fe(VI) and PMS could enhance the generation of active oxidative species, thereby improving the degradation efficiency of refractory organic pollutants (Wu et al., 2018). Given the relatively stable structure of BDE-209, it is difficult to obtain efficient degradation efficiency by a single method. It is necessary to propose a system coupling Fe(VI) and PMS for BDE-209 removal.

Thus, the main objectives of this study are to investigate the enhanced performance of Fe(VI)-PMS combined process on BDE-209 degradation. The synergistic roles of Fe(VI) and PMS were analyzed and the dominant active species were identified. The removal efficiencies and kinetics under different reaction parameters, including the dosages of Fe(VI) and PMS, the concentration of BDE-209, the initial solution pH and temperature, were comprehensively investigated. Moreover, the degradation intermediates were identified so as to propose the possible degradation mechanism of BDE-209 by Fe(VI)-PMS combined process. The toxicity variations and controlling effects of the treated water samples were further evaluated at the same time. Finally, the Fe(VI)-PMS combined process was applied to degrade BDE-209 in actual water.

2. Materials and methods

2.1. Chemicals and materials

Decabromodiphenyl ether (BDE-209, purity $\geq 98\%$, Sigma-Aldrich, USA) and ferrate(VI) (K_2FeO_4 , purity $\geq 99\%$, Sigma-Aldrich, USA) were purchased and utilized without additional purification, with the molecule structure of BDE-209 depicted in Fig. 1. Prior to the experiments, solutions of BDE-209 and ferrate(VI) with specified concentrations were prepared. The BDE-209 solution was prepared by dissolving its powder in a solvent comprising 0.5 % tetrahydrofuran, which showed negligible

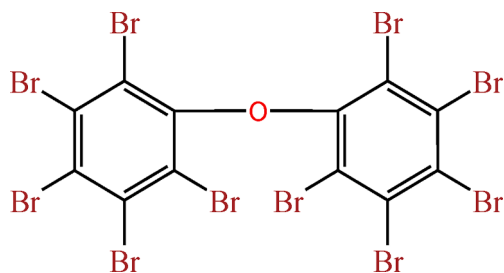


Fig. 1. The molecule structure of BDE-209.

impact on BDE-209 removal. All other chemicals and reagents employed in the experiments were of chromatographic or analytical grade. All reaction solutions were prepared with deionized and ultrapure water (Milli-Q Direct 8, USA). Luminescent bacteria (the freeze-dried bacteria *Vibrio fischeri*) used for toxicity assessment were procured from SDIX Company in the USA (DeltaTox) and stored at -20°C .

2.2. Experimental methods

2.2.1. 2.2.1 BDE-209 degradation experiments

The degradation of BDE-209 was conducted in 500 mL conical flasks. Initially, a BDE-209 solution with a concentration of $0.5\ \mu\text{mol/L}$ was introduced into the conical flask, followed by pH adjustment using either HCl or NaOH to achieve the desired value. The degradation reactions were then initiated by adding specific volumes of ferrate(VI) and PMS solutions based on the experimental conditions. At the same time, the system was stirred at 600 r/min during the reactions. At pre-determined time intervals, 20 mL samples were withdrawn and the reactions were promptly terminated with the addition of 50 μL hydroxylamine hydrochloride solution ($0.18\ \text{mol/L}$). Finally, the samples were centrifuged at 12,000 r/min for 5 min before subsequent analysis. The experimental conditions were selected basing on the existing literature and previous studies on pollutant degradation (Han et al., 2023; Helmy et al., 2021; Sboui et al., 2023). And all experiments were conducted in triplicate with the adoption of the average testing values (Helmy et al., 2021).

2.2.2. 2.2.2 free radical quenching experiments

The free radical quenching experiments were carried out by adding ethanol (EtOH) and *tert*-butanol (TBA), which have different reaction rates with $\text{SO}_4^{\bullet-}$ and $\bullet\text{OH}$. EtOH was employed as the quencher for both $\text{SO}_4^{\bullet-}$ and $\bullet\text{OH}$, whereas TBA served as the quencher specifically for $\bullet\text{OH}$. EtOH and TBA were utilized at the concentrations of $0.005\ \text{mmol/L}$, which were 10^4 times greater than that of BDE-209 and thus capable of fully quenching the free radicals during the reactions. Prior to the experiments, certain volumes of EtOH and TBA were added during the preparation of BDE-209 solution. Subsequently, the experiments were carried out following the procedures outlined in “2.2.1 BDE-209 degradation experiments”. The treated water samples were taken for analysis regularly. The removal rates of BDE-209 were compared with the control experiments conducted without the presence of quenching agents to determine the dominant species of free radicals generated in the Fe(VI)-PMS combined process.

2.2.3. 2.2.3 electron paramagnetic resonance spectroscopy (EPR) experiments

The electron paramagnetic resonance (EPR) technique was employed to directly identify the free radical species generated in the Fe(VI)-PMS combined process, a method commonly utilized in similar researches (Wu et al., 2020; Wu et al., 2019). Given the brief existence time of $\text{SO}_4^{\bullet-}$ and $\bullet\text{OH}$ in aqueous solution, 5,5-dimethyl-1-pyridine N-oxide (DMPO) was used to capture $\text{SO}_4^{\bullet-}$ and $\bullet\text{OH}$ so as to form stable products DMPO- $\text{SO}_4^{\bullet-}$ and DMPO-OH with distinctive signal peaks (Wu

et al., 2020). During the experiments, certain volumes of Fe(VI) ($0.1\ \text{mmol/L}$) and PMS ($0.1\ \text{mmol/L}$) were simultaneously added to the flask and rapidly mixed with 10 mL ultrapure water ($\text{pH} = 7.0$). Then, 20 μL of solution was withdrawn into a glass capillary and thoroughly mixed with 10 μL of DMPO solvent. Finally, the solution was subjected to EPR analysis under the following specific conditions: the central magnetic field strength, the scanning width, microwave power, microwave frequency, and the instrument scanning time were set at 350 mT, 5 mT, 0.998 mW, 9055 MHz, and 1 min, respectively.

2.3. Analytical methods

The concentration of BDE-209 was analyzed using Ultra Performance Liquid Chromatography (UPLC, Waters H-Class, USA) equipped with a BEHC18 capillary column ($250 \times 4.6\ \text{mm}$, column temperature $30\ ^{\circ}\text{C}$) and an Acquity TUV detector ($\lambda = 226\ \text{nm}$). After centrifugation at 12,000 r/min for 5 min, 1 mL of supernatant was collected. The mobile phase was 95 % methanol and 5 % ultrapure water, with a flow rate of 1 mL/min and an injection volume of 1 μL . The residual concentration of Fe(VI) was determined using the ABTS method (Han et al., 2015).

The concentrations of free bromide (Br^-) and bromate (BrO_3^-) were measured by ion chromatography (DIONEX ICS-5000, USA), equipped with a Dionex IonPac AS19 protective column ($4 \times 50\ \text{mm}$) and a Dionex IonPac AS19 analytical column ($4 \times 250\ \text{mm}$). The injection volume was 100 μL . The eluent was a KOH solution with a concentration of 100 mmol/L, flowing at a rate of 0.25 mL/min. The detailed leaching process was as follows: the initial ratio of KOH was set to be 5 % at the beginning of injection and kept for 10 min; then, the ratio gradually increased to 25 % at 25 min and maintained for 10 min; finally, the ratio was reduced to 5 % at the speed of $4\ \% \text{ min}^{-1}$ and sample injection was terminated.

The identification of organic intermediates were conducted using gas chromatography-mass spectrometry (Agilent7890A/GC-5975C MS), with detailed testing methods provided in the “Supplementary Material (Text S1)”. The solution pH was measured using a portable digital pH meter (pHS-3B, Shanghai, China).

The comprehensive biological toxicity of water samples during BDE-209 degradation was evaluated by DeltaTox II toxicity detection analyzer (DeltaTox® II, SDIX, USA), following the ISO standard luminescent bacteria toxicity test. The luminescent bacteria, known for their high sensitivity and ease of operation in toxicity detection, were commonly utilized for assessing integrated and acute toxicity (Ding et al., 2015; Sarkar et al., 2023). The specific procedures are outlined in the “Supplementary Material (Text S2)”. Toxicity test results were quantified by the relative inhibitory rate (T%) of luminescent bacteria, calculated with the formula shown below (Ding et al., 2015). The results of this method have been proved that could reflect the comprehensive toxicity of the water samples, which was caused by the target pollutants and their degradation intermediates (Sarkar et al., 2023).

$$T\% = \frac{E_0 - E}{E_0} \times 100\% \quad (1)$$

Where E_0 and E represented the initial and measured luminescence, respectively.

3. Results and discussion

3.1. Performances of different systems on BDE-209 degradation

The degradation of BDE-209 was investigated in three different oxidation systems: sole PMS oxidation, sole Fe(VI) oxidation, and Fe(VI)-PMS combined oxidation. The experiments were conducted with a BDE-209 concentration of $0.5\ \mu\text{mol/L}$, and PMS and Fe(VI) dosages of $0.1\ \text{mmol/L}$, at an initial solution pH of 7.0 and a temperature of $20 \pm 1^{\circ}\text{C}$. The BDE-209 degradation rates and the kinetics of the reactions were analyzed, as depicted in Fig. 2. From Fig. 2(a), it is evident that the Fe(VI)-PMS combined process exhibited superior efficacy in BDE-209

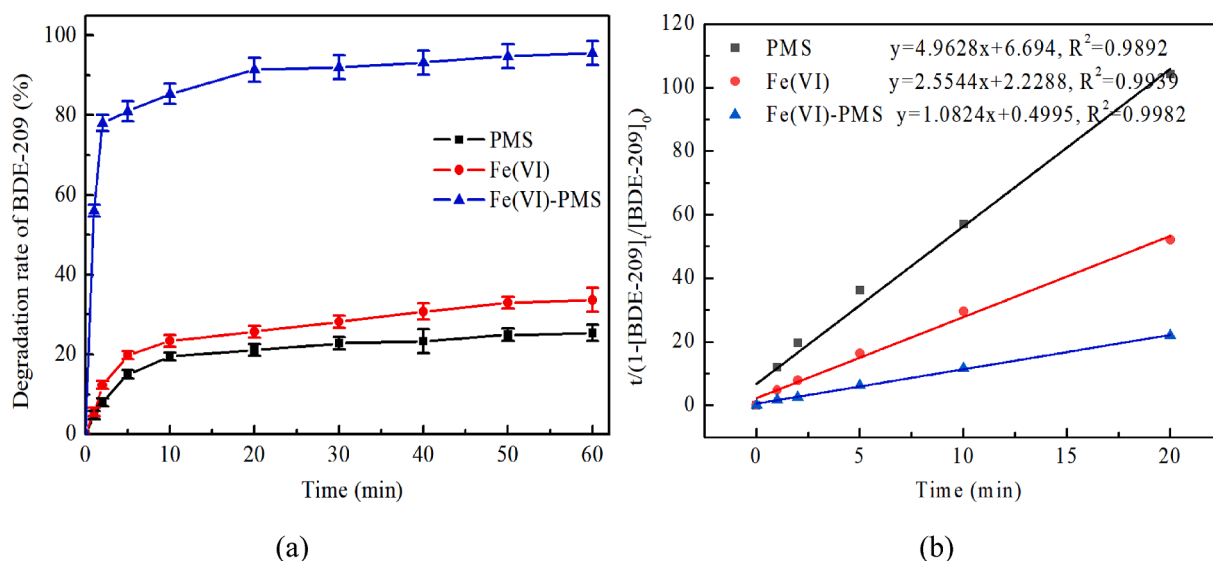


Fig. 2. Performances of different oxidation systems on BDE-209 degradation. (a) Degradation efficiency of BDE-209 in three different oxidation systems; (b) Kinetic fitting in three different oxidation systems. (Experimental conditions: $[PMS]_0 = [Fe(VI)]_0 = 0.1$ mmol/L, $[BDE-209]_0 = 0.5$ μ mol/L, initial solution pH = 7.0, temperature = 20 ± 1 °C.).

degradation compared to sole Fe(VI) and PMS oxidation process. Within 1 min of reaction, BDE-209 degradation rates were only 5.6 % and 4.8 % for sole Fe(VI) and PMS oxidation, respectively. After reaction for 60 min, the BDE-209 removal rates in the sole oxidation systems reached only 33.65 % and 25.40 %, respectively. In contrast, BDE-209 removal rates in Fe(VI)-PMS combined process (56 % and 95.6 %) were significantly higher than the cumulative rates of the two sole process (10.40 % and 59.05 %). The results suggested a synergistic effect between Fe(VI) and PMS in BDE-209 degradation. Additional experiments were conducted to obtain the optimal oxidant dosages required for complete BDE-209 removal, as detailed in Table S1. In the sole PMS and sole Fe(VI) oxidation processes, the needed concentrations of PMS and Fe(VI) were 1.0 and 0.8 mmol/L, respectively, which were reduced to 0.1 and 0.2 mmol/L in the Fe(VI)-PMS combined process, demonstrating the cost-saving advantages of this combined approach. In addition, the control experiments were carried out to assess the contribution of Fe^{3+} colloid to BDE-209 removal in the Fe(VI)-PMS combined process, depicted in Fig. S1(a). However, sole adsorption led to a mere 3.67 % total removal of BDE-209 after reaction for 60 min, indicating the limited role of Fe^{3+} colloid due to the low dosage of Fe(VI). Consequently, the degradation of BDE-209 in the Fe(VI)-PMS process was mainly by oxidation rather than adsorption.

As depicted in Fig. 2(a), the removal of BDE-209 in the three systems could be divided into two stages: an initial rapid reaction stage and a subsequent slow degradation stage. This behavior did not fit well with the first-order and second-order kinetics. Therefore, a kinetic equation capable of describing these two reaction stages is presented as Eqs. (2), which could also be reformulated to derive Eqs. (3) (Gong et al., 2020).

$$\frac{[BDE-209]_t}{[BDE-209]_0} = 1 - \frac{t}{at+b} \quad (2)$$

$$\frac{t}{1 - \frac{[BDE-209]_t}{[BDE-209]_0}} = at+b \quad (3)$$

Where t represents the reaction time (min); $[BDE-209]_t$ and $[BDE-209]_0$ represent the concentrations of BDE-209 at time t and 0 min, respectively; $1/a$ denotes the theoretical maximum removal rate of BDE-209; $1/b$ is the apparent rate constant k_{obs} (min^{-1}). With $t/(1-[BDE-209]_t/[BDE-209]_0)$ as the Y axis and t (0–20 min) as the X axis, the data was fitted to obtain the rate equation of the corresponding reaction system, as shown in Fig. 2(b) and Fig. S1(b). It can be concluded that

Eqs. (3) was well-fitted to the tendencies of BDE-209 degradation ($R^2 \geq 0.99$ in the three oxidation processes), as evidenced in other studies (Li et al., 2008; Zhang et al., 2012). The apparent rate constants k_{obs} was 2.00 min^{-1} for Fe(VI)-PMS combined process, which was respectively more than 13.33 and 4.45 times higher than that of sole PMS ($k_{obs} = 0.15 \text{ min}^{-1}$) and Fe(VI) ($k_{obs} = 0.45 \text{ min}^{-1}$) oxidation system. The results demonstrated that the Fe(VI)-PMS combined process could effectively improve the degradation rate of BDE-209. This enhancement might be attributed to the synergistic effect between PMS and Fe(VI), which promoted the generation of abundant reactive species ($SO_4^{\bullet-}$ and $\bullet OH$) for the degradation of BDE-209.

Although Fe(VI) and PMS are both strong oxidants, when used alone with low dosage, BDE-209 might be difficult to be effectively oxidized solely through direct molecular oxidation. Thus, the removal rate of BDE-209 was not satisfactory in sole Fe(VI) and PMS oxidation system. It has been identified by other studies (Han et al., 2019; Kwon et al., 2015) that during the self-decomposition of ferrate(VI), a variety of valence irons could be generated, such as Fe(V), Fe(IV), Fe(III) and Fe(II). In addition, it is well-known that PMS could be activated by various methods to generate more $SO_4^{\bullet-}$, including thermal activation, photo-activation, transition metal and metal oxide activation, etc (Bruton and Sedlak, 2018; Kwon et al., 2015; Ma et al., 2019). Among these methods, metal ion activation of persulfate exhibits higher efficiency and better pollutant removal effects. Meanwhile, metal oxide activation method has the advantages of recyclable catalyst use, absence of secondary pollution, simple operation process, and low energy requirements, making it a promising approach in water treatment (Ma et al., 2019; Ren et al., 2021). Thus, the synergistic effect observed in the Fe(VI)-PMS combined process might be attributed to the iron intermediates of Fe(VI), which could effectively activate PMS to form more $SO_5^{\bullet-}$ and $SO_4^{\bullet-}$, as expressed in formulas (4)-(5) (Sun et al., 2018).



3.2. Identification of the dominant active species for BDE-209 degradation

In this study, the dominant active species were identified through free radical quenching experiments and electron paramagnetic

resonance spectroscopy (EPR) experiments. Previous research has shown that the maximum reaction rate constant between tertiary butanol (TBA) and $\bullet\text{OH}$ was $7.6 \times 10^8 \text{ M}^{-1}\text{s}^{-1}$, which was 10^3 times higher than that of TBA with $\text{SO}_4^{\bullet-}$ ($9.1 \times 10^5 \text{ M}^{-1}\text{s}^{-1}$) (Dong et al., 2019). Comparatively, the reaction rate constants of ethanol (EtOH) with $\bullet\text{OH}$ and $\text{SO}_4^{\bullet-}$ were in the ranges of 1.2×10^9 – 2.8×10^9 and 1.6×10^7 – $7.7 \times 10^7 \text{ M}^{-1}\text{s}^{-1}$, respectively (Wu et al., 2020). Thus, TBA could effectively quench $\bullet\text{OH}$, while EtOH could quench both $\bullet\text{OH}$ and $\text{SO}_4^{\bullet-}$. In the Fe(VI)-PMS combined process, PMS may be activated by Fe(VI) intermediates to generate more free radicals such as $\bullet\text{OH}$ and $\text{SO}_4^{\bullet-}$ for BDE-209 degradation. In order to identify the roles of these free radicals and determine the dominant species responsible for BDE-209 degradation, radical quenching experiments were carried out by dosing excessive quenching agents TBA and EtOH, with a molar ratio of TBA and EtOH to BDE-209 both setting at 10000:1. The corresponding BDE-209 degradation efficiencies and reaction kinetics under three different conditions were analyzed, as depicted in Fig. 3(a)–(b) and Fig. S2.

As shown in Fig. 3(a), the removal rate of BDE-209 was significantly decreased from 95.6 % to 51.65 % after addition of TBA. Meanwhile, when EtOH was employed as a radical scavenger, the degradation efficiency of BDE-209 was kept at 25.68 % after reaction for 60 min, which was 26 % lower than that in the TBA-added oxidation system. Comparatively, the degradation of BDE-209 was enhanced by 61.95 % when PMS was combined with Fe(VI) oxidation system. These results suggested that both $\bullet\text{OH}$ and $\text{SO}_4^{\bullet-}$ were generated and participated in the degradation of BDE-209 in the Fe(VI)-PMS combined process. Furthermore, it also confirmed that $\bullet\text{OH}$ was the dominant active species contributing to the oxidation removal of BDE-209 in the coupled Fe(VI)-PMS system. Additionally, the enhanced generation of $\text{SO}_4^{\bullet-}$ also played a significant role in the promoted removal of BDE-209 in the combined system. Moreover, as seen from the results of the EPR experiments (Fig. S3), respectively four characteristic peaks with an intensity ratio of 1:2:2:1 and six characteristic peaks with an intensity ratio of 1:1:1:1:1:1 were clearly achieved, corresponding to the characteristic peaks of $\bullet\text{OH}$ and $\text{SO}_4^{\bullet-}$. The results further directly confirmed the presence of $\bullet\text{OH}$ and $\text{SO}_4^{\bullet-}$, consistent with findings reported in other studies (Giannakis et al., 2021; Xiong et al., 2021; Su et al., 2022).

The contributions of each free radical species could also be distinguished by changes in reaction kinetics and the reaction rate constants, as illustrated in Fig. 3(b) and Fig. 2S, respectively. In general, the rate constants k_{obs} of the reaction system were significantly reduced with the addition of TBA and EtOH. Specifically, the value of k_{obs} decreased from

2.0 min^{-1} in Fe(VI)-PMS combined process to 0.19 and 0.09 min^{-1} , respectively, in the EtOH and TBA added process, representing a reduction by at least 10.53 times. This results further proved that the reduction of active species ($\bullet\text{OH}$ and $\text{SO}_4^{\bullet-}$) in the oxidation system led to the decrease in BDE-209 removal rate, with $\bullet\text{OH}$ being the dominant species.

3.3. Effects of experimental parameters on the degradation of BDE-209

The factors influencing the degradation efficiencies of BDE-209 by Fe(VI)-PMS combined process was systematically investigated in this study, including Fe(VI) dosage (0.1–0.5 mmol/L), PMS dosage (0.1–0.5 mmol/L), initial solution pH (3.0–11.0), temperature (10–40 °C) and BDE-209 concentration (0.1–5.0 $\mu\text{mol/L}$), with the degradation rates of BDE-209 and the reaction kinetics being analyzed.

3.3.1. Effect of Fe(VI) dosage

As shown in Fig. 4(a), the increase of Fe(VI) dosage was beneficial to BDE-209 removal during the Fe(VI)-PMS oxidation process. The degradation rate of BDE-209 significantly increased from 62.65 % to 100 % as the Fe(VI) dosage gradually increased from 0.01 to 0.2 mmol/L. The reaction time required for complete removal of BDE-209 decreased from 20 to 10 min when the Fe(VI) dosage further increased to 0.5 mmol/L. In addition, the oxidation reactions were well fitted with the kinetic equation (3) at different Fe(VI) dosages ($R^2 \geq 0.993$), as illustrated in Fig. S4(a). Correspondingly, the apparent rate constant k_{obs} noticeably increased from 0.51 to 4.50 min^{-1} by increasing the Fe(VI) dosage from 0.01 to 0.5 mmol/L, as shown in Fig. 4(b). The results indicated that more active species were generated in the system with the increase in the Fe(VI) dosage, thereby promoting the degradation of BDE-209 and accelerating the reaction rate. As the Fe(VI) dosage increased, more intermediate valence irons (such as Fe(V), Fe(IV), Fe(III) and Fe(II)) were generated (Han et al., 2018; Han et al., 2019), promoting the production of more $\bullet\text{OH}$ and $\text{SO}_4^{\bullet-}$ and enhancing the degradation of BDE-209. However, in view of the high pharmaceutical cost of Fe(VI), 0.1 mmol/L was chosen as the appropriate dosage for the subsequent investigations of the Fe(VI)-PMS combined process.

3.3.2. Effect of PMS dosage

As the only source of $\text{SO}_4^{\bullet-}$ in the reaction system, the dosage of PMS significantly affects the generation of active substances, thereby directly impacting the removal of BDE-209 in the Fe(VI)-PMS combined process.

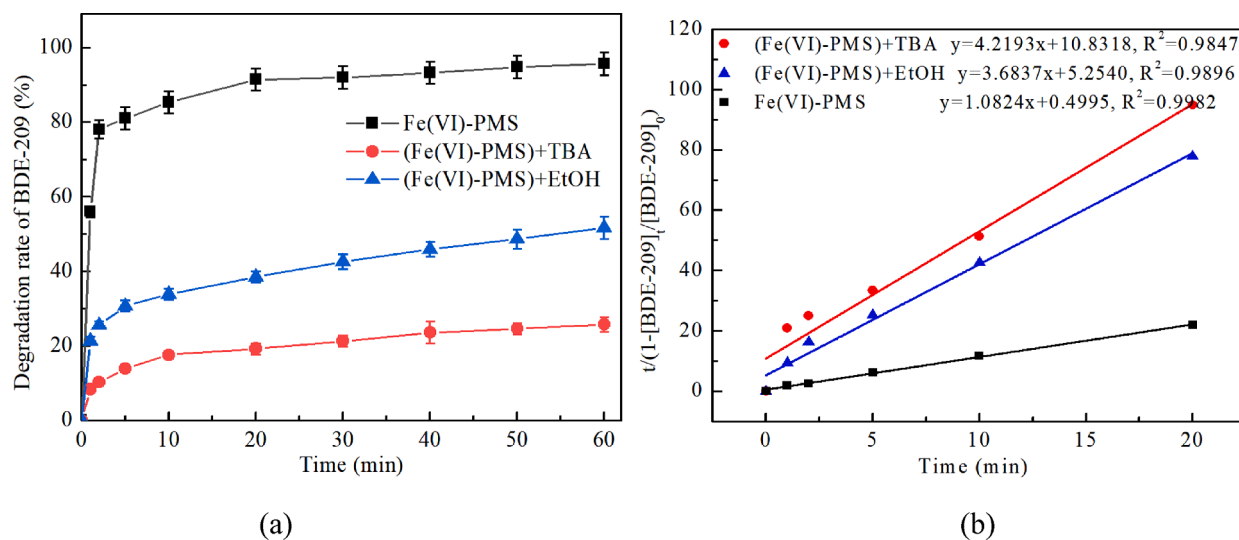


Fig. 3. Identification of the dominant active species by the free radical quenching experiments in Fe(VI)-PMS combined process. (a) Degradation efficiency of BDE-209; (b) Reaction kinetics fitting in the free radical quenching experiments. (Experimental conditions: $[\text{PMS}]_0 = [\text{Fe(VI)}]_0 = 0.1 \text{ mmol/L}$, $[\text{BDE-209}]_0 = 0.5 \mu\text{mol/L}$, $[\text{TBA}]_0 = [\text{EtOH}]_0 = 0.005 \text{ mmol/L}$; initial solution pH = 7.0, temperature = $20 \pm 1^\circ\text{C}$.)

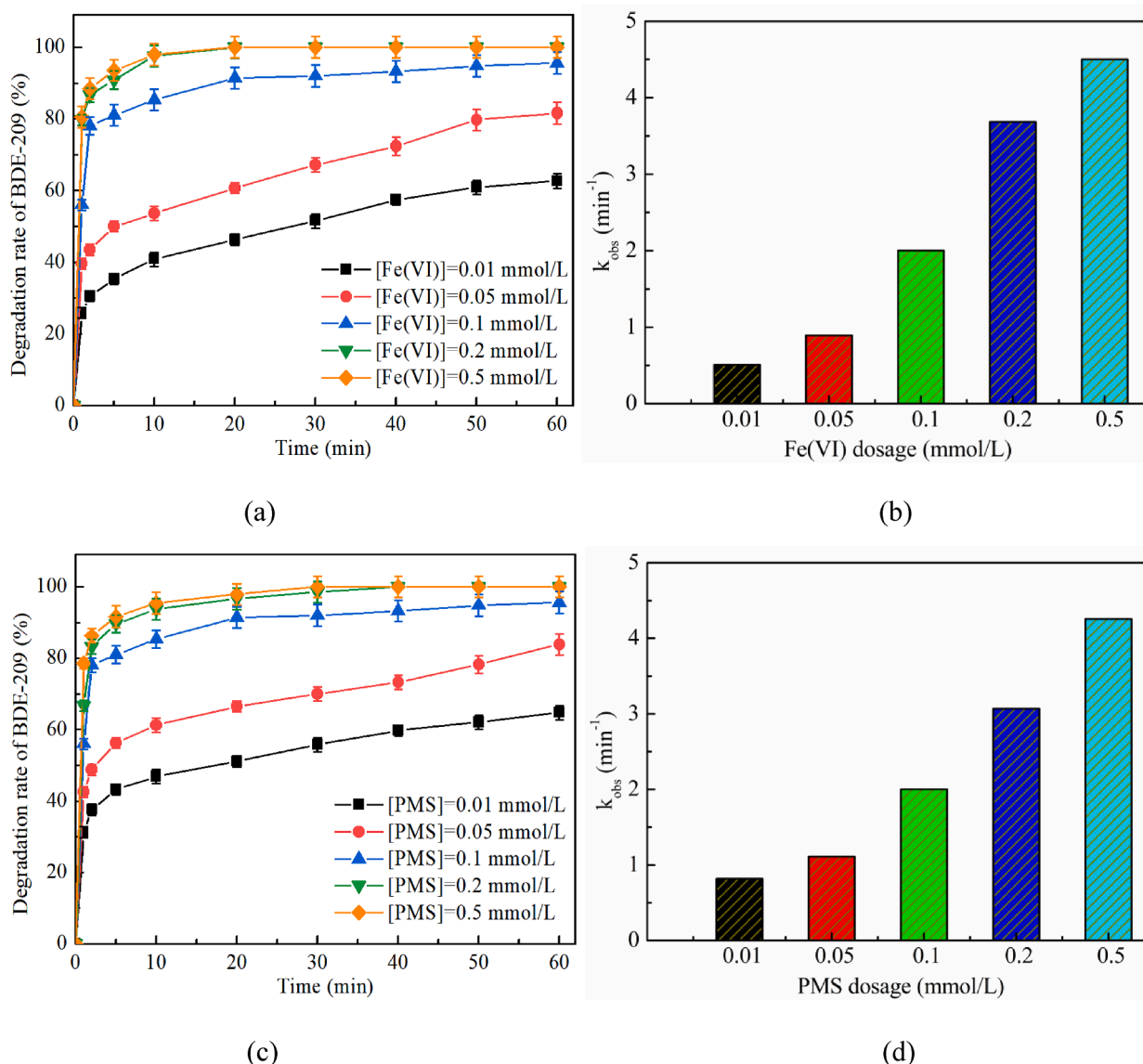
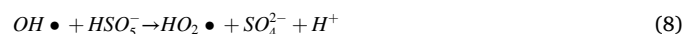


Fig. 4. Effects of Fe(VI) and PMS dosages on BDE-209 degradation rates ((a) and (c)) and reaction kinetics ((b) and (d)). (Experimental conditions: $[BDE-209]_0 = 0.5 \mu\text{mol/L}$; $[Fe(VI)]_0 = 0.01\text{--}0.5 \text{ mmol/L}$ for (a) and (b), 0.1 mmol/L for (c) and (d); $[PMS]_0 = 0.01\text{--}0.5 \text{ mmol/L}$ for (c) and (d), 0.1 mmol/L for (a) and (b); initial solution pH = 7.0, temperature = $20 \pm 1^\circ\text{C}$).

Fig. 4(c) and (d) have depicted the influences of different PMS dosages (0.01–0.5 mmol/L) on BDE-209 removal rates and the reaction kinetics within 60 min. Similar to Fe(VI) dosage, the increase of PMS dosage could significantly improve the removal rate of BDE-209 by Fe(VI)-PMS combined process, which increased notably from 64.75 % to 100 % with PMS dosing ranging from 0.01 to 0.2 mmol/L. The time required for complete removal of BDE-209 decreased from 30 to 20 min as the PMS dosage increased from 0.2 to 0.5 mmol/L. Additionally, the oxidation reactions under different PMS dosages were also well fitted with the kinetic equations (as shown in Fig. S4(b) and Fig. 4(d)), with the values of k_{obs} significantly increasing from 0.82 to 4.26 min^{-1} with PMS dosing from 0.01 to 0.5 mmol/L.

When the dosage of PMS was low, the amount of PMS available for activation was limited, resulting in the relatively restricted production of $\bullet\text{OH}$ and $\text{SO}_4^{\bullet-}$ []. Consequently, BDE-209 could not be effectively degraded with low PMS dosage, which was reflected in the low removal rates and reaction rate constants. By increasing the PMS dosage, the amount of activated PMS gradually increased, generating more active substances and enhancing the oxidative capacity of the Fe(VI)-PMS combined process. Thus, the degradation of BDE-209 was improved

with the increase of PMS dosage. However, excessive PMS dosage might lead to the scavenging effect of reactive oxygen species (ROS) and the production of low reactive radicals and excessive SO_4^{2-} (as described in Eqs.(6–8) (Chen et al., 2018)). Therefore, 0.1 mmol/L PMS was chosen as the optimum dosage, under which 95.6 % removal of BDE-209 was achieved.



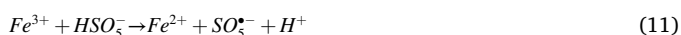
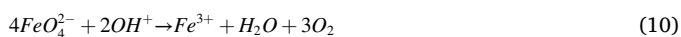
3.3.3. Effect of initial pH

It is well known that the initial pH of the solution plays a crucial role in the application of advanced oxidation technology for wastewater treatment, as it significantly influences the generation of free radicals and the removal efficiencies of pollutants (Kuo et al., 2012). Combined

with the practical water treatment, five different initial pH values (3.0, 5.0, 7.0, 9.0, 11.0) were chosen to investigate their effects on the removal of BDE-209 by Fe(VI)-PMS combined process, with the results presented in Fig. 5(a) and (b).

As depicted in Fig. 5(a), the degradation performance was highly dependent on initial pH values. The removal rate of BDE-209 increased significantly from 72.35 % to 97.95 % within 60 min as the initial pH was raised from 3.0 to 5.0. However, as the pH value continued to increase from 7.0 to 11.0, the removal rate of BDE-209 dramatically decreased from 95.6 % to 48.75 %. The results indicated that the strong acid-base environment was not conducive to the degradation of BDE-209. Nevertheless, an over 85 % degradation rate of BDE-209 was obtained within a wide range of initial pH values (5.0–9.0), demonstrating the strong adaptability of Fe(VI)-PMS combined process to varying initial pH conditions. Regarding the reaction kinetics, the degradation reactions of BDE-209 were well described by the kinetic equation (3) under different pH conditions ($R^2 \geq 0.996$), as illustrated in Fig. S5(a) and Fig. 5(b). The maximum rate constant k_{obs} of Fe(VI)-PMS oxidation process was 2.80 min^{-1} under an initial pH of 5.0. However, when initial pH was lower than 3.0 or higher than 11.0, the corresponding values of k_{obs} were both significantly decreased to 1.73 or even 0.47 min^{-1} .

On the one hand, the initial pH might influence the transformations of the dominant Fe(VI) species. According to the reported researches (Han et al., 2018), the main species of Fe(VI) included H_3FeO_4^+ , H_2FeO_4 , HFeO_4^- and FeO_4^{2-} , which inter-converted at different pH values ($\text{H}_3\text{FeO}_4^+ = \text{H}_2\text{FeO}_4 + \text{H}^+$, $pK_1 = 1.6$; $\text{H}_2\text{FeO}_4 = \text{HFeO}_4^- + \text{H}^+$, $pK_2 = 3.5$; $\text{HFeO}_4^- = \text{FeO}_4^{2-} + \text{H}^+$, $pK_3 = 7.23$) (Han et al., 2019). Under strong alkaline conditions, Fe(VI) remains stable and is not readily reactive with pollutants. Within the pH range of 3.5–7.23, HFeO_4^- was the dominant active species, exhibiting stronger oxidizing ability than FeO_4^{2-} . Moreover, in the acidic and neutral solutions, FeO_4^{2-} undergoes hydrolysis to form Fe^{3+} , which could react with HSO_5^- to produce Fe^{2+} and further activate PMS to form active species (such as SO_5^{\bullet} and SO_4^{\bullet}), as illustrated in formula (10)–(12) (Gong et al., 2020; Li et al., 2019); thereby resulting in high removal efficiency of BDE-209. However, in strong alkaline conditions, $\text{Fe}^{2+}/\text{Fe}^{3+}$ were prone to deactivation due to the formation of hydroxide precipitation, leading to the dramatic decrease in the BDE-209 degradation rate.



On the other hand, as the pK_1 and pK_2 of PMS were respectively 0.0 and 9.4, thus HSO_5^- was the predominant form in the pH range of 3.0–9.0. Under the strongly acidic conditions ($\text{pH} \leq 3.0$), the hydrolysis of PMS was promoted to generate abundant hydrogen ion (H^+), which could form hydrogen bonds with HSO_5^- (Wu et al., 2018). Thus, the activation of PMS by Fe^{2+} or Fe^{3+} was hindered, leading to a reduction in the removal rate of BDE-209. In addition, SO_4^{\bullet} underwent the self-quenching reactions under acidic conditions ($\text{SO}_4^{\bullet} + \text{SO}_4^{\bullet} \rightarrow \text{S}_2\text{O}_8^{2-}$), further diminishing the oxidative capability of the Fe(VI)-PMS combined process. As the initial pH increased, more $\bullet\text{OH}$ could be formed through reactions between SO_4^{\bullet} with OH^- ($\text{SO}_4^{\bullet} + \text{OH}^- \rightarrow \text{SO}_4^{2-} + \text{OH}^{\bullet}$) (Wang et al., 2020), which was conducive to the degradation of BDE-209. Therefore, the highest removal efficiency and optimal rate constant were achieved at pH values of 5.0 and 7.0 (Fig. 5(a) and (b)). However, under strongly alkaline conditions, the conversion of $\text{Fe}^{2+}/\text{Fe}^{3+}$ was limited, resulting in the fewer newly formed SO_4^{\bullet} , which contributed to the decrease in the removal rate of BDE-209 in Fe(VI)-PMS combined process.

In addition, the pH value of the reaction system was also influenced by Fe(VI) and PMS, as shown in Fig. S6. Due to the rapid consumption of Fe(VI) during reactions, the solution alkalinity could be enhanced as

$\text{Fe}^{2+}/\text{Fe}^{3+}$ activating PMS to generate OH^- (Gong et al., 2020). The final pH of the reaction system slightly increased when the initial pH of solution was acidic. For example, when the initial pH was 3.0 and 5.0, the corresponding final pH was 3.65 and 6.52, respectively. However, the final pH decreased to 7.23 and 9.85 for initial pH values of 9.0 and 11.0, respectively, which might be caused by the increased formation of Fe(OH)₃ in the alkaline solution. Considering both the solution pH and the BDE-209 removal rate, an initial pH of 7.0 was chosen as the optimal condition in this study.

3.3.4. Effect of temperature

The impact of temperature on the degradation of BDE-209 was assessed in the range of 10 ~ 40 °C, with the results presented in Fig. 5 (c)–(d) and Fig. S5(b). It was evident that at lower temperatures, such as 10 °C, the oxidation reactions in the Fe(VI)-PMS combined process were insufficient, resulting in a removal rate of only 62.35 % and a reaction rate constant k_{obs} of 0.61 min^{-1} . As reported (Wang et al., 2020), the viscosity coefficient of the reaction system is relatively high at lower temperatures, leading to decreased activities and effective collision frequencies between the oxidants and pollutant, thus resulting in a lower degradation efficiency of BDE-209. However, a moderate increase in temperature could gradually promote the decomposition of Fe(VI), generating more reactive species responsible for BDE-209 degradation. In addition, it could also increase the effective collision frequencies between oxidizing substances (including Fe(VI), PMS, $\bullet\text{OH}$ and SO_4^{\bullet}) and BDE-209, which was beneficial to the degradation of BDE-209 by Fe(VI)-PMS combined process. Therefore, the removal efficiency of BDE-209 gradually increased with the temperature rising from 10 to 30 °C. A 100 % removal of BDE-209 was obtained after 60 min reaction at 30 °C, with the corresponding k_{obs} as high as 2.19 min^{-1} .

However, as the temperature was too high (up to 40 °C), both the degradation rate of BDE-209 and the value of k_{obs} decreased to 89.65 % and 1.65 min^{-1} , respectively. This decline might be attributed to the reduction in Fe(VI) stability and aggravation of Fe(VI) self-decomposition, which was detrimental to BDE-209 removal. Controlled experiments were carried out for investigating the decomposition of Fe(VI) under different temperatures. The residual concentration of Fe(VI) was tested by the ABTS method (Han et al., 2015), and the result was shown in Fig. S7. The percentage of residual Fe(VI) concentration gradually decreased by increasing temperature. When the temperature increased from 10 to 40 °C, the residual Fe(VI) in water decreased from 79.75 % to 42.10 % after 60 min. Due to the fixed dosage of Fe(VI) before reactions, excessive temperature elevation would promote the self-decomposition of Fe(VI) to generate Fe(III) hydroxide oxide, which thereby weakening the oxidizing ability of Fe(VI) and hindering the degradation of BDE-209 (Yunho et al., 2005; Wagner et al., 1952). Considering the achievement of high BDE-209 removal rates (89.65 %–100 %) within the temperature range of 20–40 °C, the Fe(VI)-PMS combined process could be considered as an impressive technology for BDE-209 degradation.

3.3.5. Effect of BDE-209 concentration

Fig. 5 (e) and (f) showed the impact of BDE-209 concentration on its degradation efficiency and reaction kinetics. BDE-209 could be completely degraded when its concentration was 0.1 and 0.2 $\mu\text{mol/L}$, with the reaction rate constant k_{obs} being 3.57 and 2.90 min^{-1} , respectively. However, as the concentration of BDE-209 further increased from 0.5 to 5.0 $\mu\text{mol/L}$, the removal rate of BDE-209 gradually decreased from 95.6 % to 76.66 %. At the same time, the corresponding value of k_{obs} decreased from 2.0 to 0.58 min^{-1} . Theoretically, with constant dosages of Fe(VI) and PMS in the Fe(VI)-PMS oxidation process, the total amount of generated active species was relatively fixed before the reactions. With the increase of initial concentration of BDE-209, the molar ratio of active species to BDE-209 decreased, leading to a decrease in the degradation efficiency of BDE-209 within a specific reaction time. In order to obtain the required concentration of oxidants (Fe(VI) = PMS)

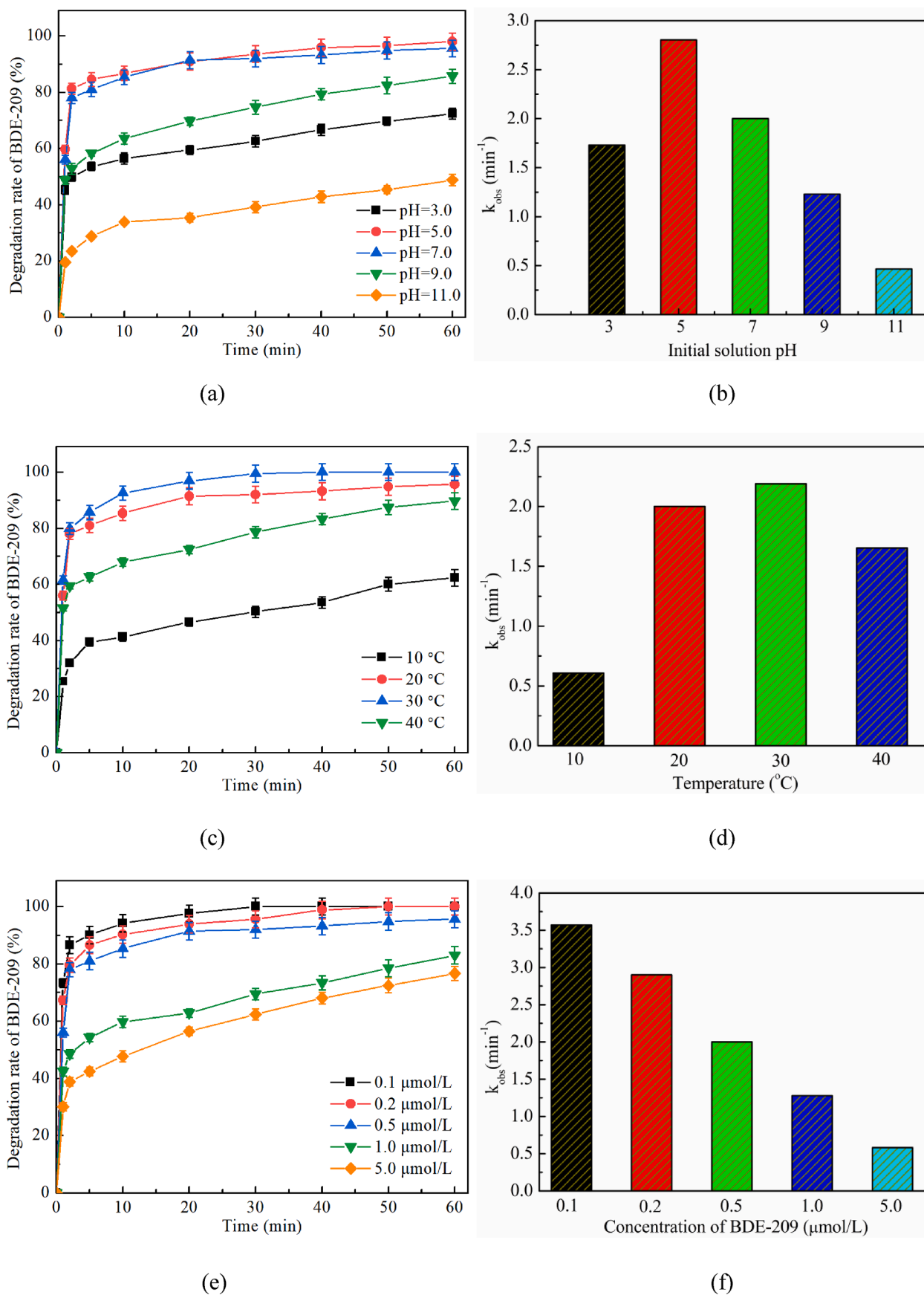


Fig. 5. Effects of initial solution pH, temperature and BDE-209 concentration on BDE-209 degradation rates ((a), (c) and (e)) and reaction kinetics ((b), (d) and (f)). (Experimental conditions: $[\text{Fe}(\text{VI})]_0 = [\text{PMS}]_0 = 0.1 \text{ mmol/L}$; initial solution pH = 7.0 for (c)-(f), 3.0–11.0 for (a) and (b); temperature = $20 \pm 1 \text{ }^\circ\text{C}$ for (a)-(b) and (e)-(f), 10–40 $^\circ\text{C}$ for (c) and (d); $[\text{BDE-209}]_0 = 0.5 \text{ } \mu\text{mol/L}$ for (a)-(d), 0.1–5.0 $\mu\text{mol/L}$ for (e) and (f)).

for complete removal of BDE-209, experiments were carried out for BDE-209 absolute degradation, as shown in Fig. S8. It was observed that the complete removal of BDE-209 could be achieved by increasing the dosage of oxidants. When the concentrations of BDE-209 were 0.1, 0.2, 0.5, 1.0 and 5.0 $\mu\text{mol/L}$, the correspondingly required concentrations of Fe(VI) and PMS for absolute degradation were 0.1, 0.1, 0.15, 0.17 and 0.65 mmol/L, respectively.

3.4. Identification of intermediates and speculation of the possible mechanisms

The identification of intermediates including the inorganic and organic ones during the degradation of BDE-209 by Fe(VI)-PMS combined process was evaluated in this study. The experimental conditions included 0.5 $\mu\text{mol/L}$ BDE-209, 0.1 mmol/L each of Fe(VI) and PMS, an initial solution pH of 7.0 and a temperature of $20 \pm 1^\circ\text{C}$. Based on the identification of intermediates, potential mechanisms were proposed.

3.4.1. Variation of inorganic products during the degradation of BDE-209

The concentrations of free bromide (Br^-) and bromate (BrO_3^-) were measured by ion chromatography as the inorganic products. The organic bromine contents both in residual BDE-209 and the organic intermediates were calculated according to the removal rate of BDE-209. Then, the variation of the Br element contents during the degradation process of BDE-209 was evaluated, as shown in Fig. 6.

In general, the total Br content remains constant throughout the degradation process. After reaction for 60 min, the removal rate of BDE-209 reached 95.60 %, with a generated Br^- concentration of 0.279 $\mu\text{mol/L}$. As the reactions progressed, the corresponding proportion of free bromide gradually increased from 0 to 66.87 % within 60 min, while the bromine content in residual BDE-209 decreased from 100 % to 4.4 %. The debromination rate in the Fe(VI)-PMS oxidation system is significantly higher compared other methods such as UV/ SO_3^{2-} advanced reduction method (20 %–30 %) and BC-nZVI/PS system (5 %–10 %) (Li et al., 2019). Moreover, no bromate was detected during the process of BDE-209 degradation by Fe(VI)-PMS combined process, similar to findings in the Fe(VI)-ozone combined process (Han et al., 2018), indicating the environmental friendly property of this technology. The bromine content in the organic intermediates initially increased to a peak value of 49.02 % within 20 min, then decreased to 28.73 % at 60 min. From the balance of the bromine content during the reaction process, it could be inferred that during BDE-209 degradation in the Fe(VI)-PMS combined process, bromine was removed from the molecular

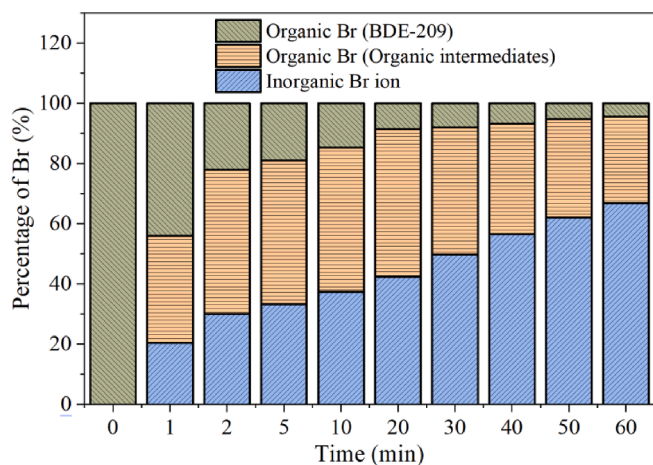


Fig. 6. Variations of Br element contents during the process of BDE-209 degradation by Fe(VI)-PMS combined process. (Experimental conditions: $[\text{PMS}]_0 = [\text{Fe(VI)}]_0 = 0.1 \text{ mmol/L}$, $[\text{BDE-209}]_0 = 0.5 \mu\text{mol/L}$, initial solution pH = 7.0, temperature = $20 \pm 1^\circ\text{C}$).

structure of BDE-209 to generate lower brominated organic intermediates at the beginning of the degradation reactions (Gong et al., 2020). As the oxidation reactions progress, the organic intermediates were further degraded to form more free bromide ions.

3.4.2. Generation of organic intermediates and mineralization effect

In order to further analyze the possible degradation mechanism of BDE-209 by Fe(VI)-PMS combined process, the generation of organic intermediates was detected by GC-MS/MS (For detailed information, refer to the “Supplementary Material (Text S1)”). Table 1 has summarized the mass spectra data of intermediate products, including retention time, molecular weight, main detected fragment ions (m/z) and molecular structure, in comparison to the NIST (National Institute of Standards and Technology) Mass Spectrometry Database and published researches. Fig. S9 has depicted the spectrum of the identified intermediates.

In this study, six degradation products have been identified by GC-MS/MS, labeled as products A-F, respectively. Generally, the lower brominated intermediates were considered as the primary products of BDE-209, which similar conclusions have also been achieved in other studies (Cheng et al., 2021; Chang et al., 2021; Zhao et al., 2021). Among these intermediates, product B (BDE-203, oct-BDE) and C (BDE-99, hepta-BDE) were considered as the main stepwise debrominated products of BDE-209, which have also been detected by other researches (Chang et al., 2021; Wu et al., 2020). However, the completely debrominated product diphenyl ether was not observed in this study. Instead, it was worth noting that the dibromo intermediates with a single aromatic ring have been identified, such as product D (2,3-dibromo-4-hydroxy-5-methoxybenzaldehyde) and E (2,3-dibromo-4-hydroxy-5-methoxybenzaldehyde). In addition, the small molecule (product F, maleic acid) which has been completely debrominated and ring cracked was also obtained in this study, indicating the efficient oxidizing performance of Fe(VI)-PMS combined process. This conclusion was further supported by the mineralization of BDE-209 by the three systems (as illustrated in Fig. 7). The mineralization rates of BDE-209 in the sole PMS and Fe(VI) oxidation processes were 5.5 % and 8.3 %, respectively. While up to 56.7 % mineralization rate was obtained in the Fe(VI)-PMS combined process, which was much higher than sum of the two sole methods (13.8 %). The results demonstrated that the Fe(VI)-PMS combined process had strong synergistic effect between two oxidants during oxidation and mineralization of BDE-209.

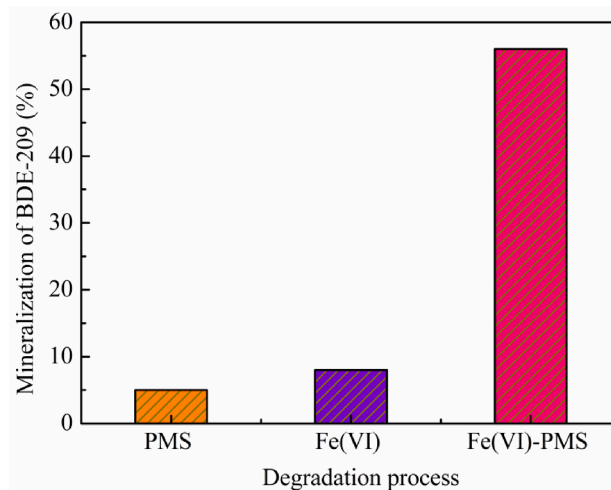


Fig. 7. Mineralization of BDE-209 in the three oxidation systems. (Experimental conditions: $[\text{PMS}]_0 = [\text{Fe(VI)}]_0 = 0.1 \text{ mmol/L}$, $[\text{BDE-209}]_0 = 0.5 \mu\text{mol/L}$, initial solution pH = 7.0, temperature = $20 \pm 1^\circ\text{C}$, reaction time = 60 min.).

3.4.3. Speculation of the degradation pathways

Based on the inorganic and organic products, the possible degradation pathways of BDE-209 by Fe(VI)-PMS combined process were proposed, as illustrated in Fig. 8. The total degradation of BDE-209 by Fe(VI)-PMS combined process might involved debromination, radical addition, substitution, beta scission, and oxidation processes, etc (Chang et al., 2021; Ma et al., 2021; Shi et al., 2021).

Firstly, BDE-209 underwent stepwise debromination reactions by free radicals ($\text{SO}_4^{\cdot-}$ and $\cdot\text{OH}$), resulting in the formation of lower brominated congeners and free bromine. This stepwise debromination of BDE-209 was accomplished by gradually replacing bromine atoms with hydrogen atoms so as to generate a series of BDEs with lower bromine numbers, such as nona-BDE, octa-BDE, hepta-BDE, etc. Then, the debromination products were attacked by free radicals and other active species to make them oxidatively degraded. The cleavage of the C-O bond linking two benzene rings occurred through a combination of addition, elimination and substitution, yielding low-brominated intermediates with a single benzene ring structure, exemplified by products D and E. The debromination reactions continued during the above process. In addition, the hydroxylation, beta scission, ring-opening and other reactions were happened to generate lower molecular product (such as maleic acid), which were further completely oxidized and mineralized to CO_2 and H_2O .

3.5. Toxicity control

The toxicities of BDE-209 and its debrominated products formed via biodegradation have been assessed in several studies (Yu et al., 2020; Yu et al., 2019). It has been identified that the intermediates generated during BDE-209 degradation may exhibit higher toxicity than BDE-209, potentially posing ecological risks (Tiwari et al., 2017). Therefore, in this study, variations in the toxicity of the water samples during BDE-209 degradation process were evaluated through luminescent bacteria toxicity test, and the results were presented in Fig. 9.

Overall, the comprehensive toxicity levels peaked within the initial

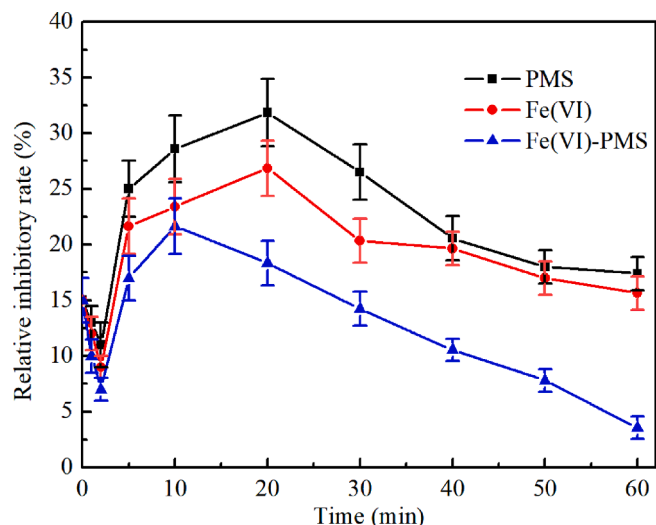


Fig. 9. Analysis of the biotoxicity during BDE-209 degradation process. (Experimental conditions: $[\text{PMS}]_0 = [\text{Fe(VI)}]_0 = 0.1 \text{ mmol/L}$, $[\text{BDE-209}]_0 = 0.5 \mu\text{mol/L}$, initial solution pH = 7.0, temperature = $20 \pm 1^\circ\text{C}$.)

10 or 20 min in all three oxidation systems. The initial relative inhibitory rate (T%) was 15.0 %, indicating the moderate toxicity of BDE-209. However, the maximum T% values observed in the processes of sole PMS oxidation, sole Fe(VI) oxidation, and the Fe(VI)-PMS combined process were 31.85 % (20 min), 26.86 % (20 min) and 21.65 % (10 min), respectively. The increase of toxicity could be attributed to the formation and accumulation of more toxic intermediates, such as stepwise debrominated ones, dibromo ones, phenolic ones, etc (Cheng et al., 2021; Zhu et al., 2022). In this study, the detected debrominated products of BDE-209 were product B (BDE-203, oct-BDE) and C (BDE-99, hepta-BDE), which had been proved to have higher propagation and growth toxicities than BDE-209 (Tan et al., 2017). With further

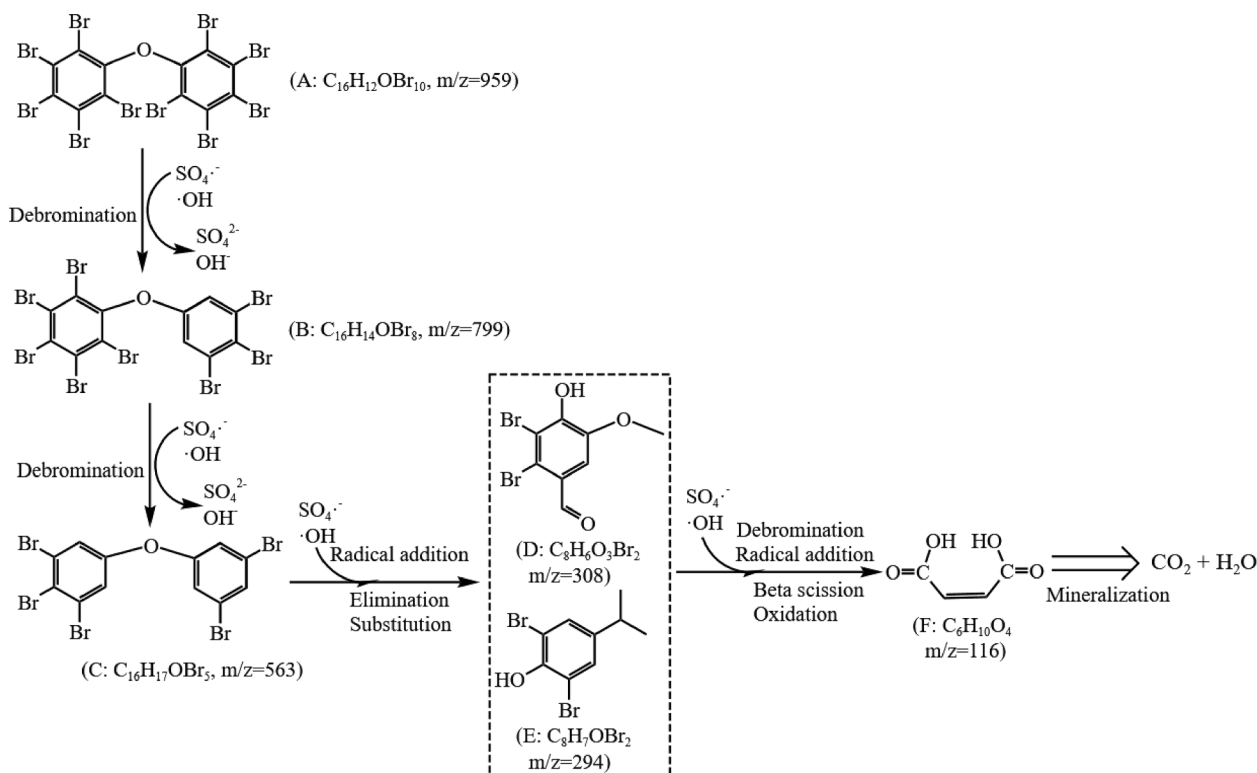


Fig. 8. Degradation pathways of BDE-209 in Fe(VI)-PMS combined process.

oxidation of BDE-209 and its intermediates, the relative inhibitory rates of the water samples to luminescent bacteria gradually decreased in all three systems, reflecting the controlling effects of the toxicities. Notably, the Fe(VI)-PMS combined process showed a better controlling role on the toxicity than the other two sole oxidation processes. At the end of degradation (60 min), the T% values in both sole PMS and Fe(VI) oxidation processes were still as high as 17.4 % and 15.65 %, respectively, which was close to that of BDE-209 itself (15 %). However, the relative inhibition rate in Fe(VI)-PMS combined process was only 3.56 %, indicating the much lower toxicity than BDE-209. In summary, these findings underscored the faster and stronger capability of the Fe(VI)-PMS combined process in controlling the comprehensive toxicity compared to the two sole oxidation process.

Similar results have been reported in other studies (Tan et al., 2017; Davies and Zou, 2012), where greater toxic intermediate products were generated in the reductive debromination process of BDE-209. The reductive intermediate products had higher toxicities in both *Daphnia magna* and *Microcystis flos-aquae* than BDE-209 itself. However, the toxicity could be reduced if the reductive debromination process was completely conducted. Moreover, the toxicity could even be eliminated if the reductive process was followed by subsequent oxidative degradation.

3.6. Degradation of BDE-209 by Fe(VI)-PMS combined process in actual water

To investigate the efficacy of the Fe(VI)-PMS combined process in removing BDE-209 from actual water sources, experiments were carried out using laboratory tap water and water from the Maozhou river (Shenzhen, Guangdong, China). The water quality parameters of the Maozhou river were detailed in Table S2 and the results were illustrated in Fig. 10. As seen from Fig. 10(a), compared with the effective degradation of BDE-209 in solution prepared by ultrapure water, the removals of BDE-209 in tap water and Maozhou river were obviously inhibited. After contacting reaction for 60 min, the degradation efficiency of BDE-209 decreased significantly from 95.6 % to 52.65 % (in tap water) and 43.44 % (in the Maozhou river). This inhibition might be caused by the coexisting ions in actual waters, such as CO_3^{2-} , NO_3^- , PO_4^{3-} , NH_4^+ and NOM, which could compete with BDE-209 for the consumption of free radicals

($\text{SO}_4^{\cdot-}$ and $\bullet\text{OH}$) (Graham et al., 2004). Consequently, the rapid depletion of oxidizing species directly resulted in the deterioration of BDE-209 degradation. However, increasing the dosages of the oxidants (Fe(VI) and PMS) could ameliorate these inhibitory effects, ensuring sufficient BDE-209 removal. As illustrated in Fig. 10(b), as the concentrations of Fe(VI) and PMS increased to 4 times of the base dosages ($C = 4C_0 = 0.4 \text{ mmol/L}$), the removal rate of BDE-209 significantly increased to 100 % and 81.56 % in tap water and Maozhou river, respectively. In addition, as high as 95.35 % removal rate of BDE-209 was also achieved in Maozhou river system by increasing the dosages of oxidants to 5 times ($C = 5C_0 = 0.5 \text{ mmol/L}$). In summary, the application of actual water showed that Fe(VI)-PMS combined process was a perspective technology for effective removal of pollutants. However, given the small-scale nature of the experiments, further expansion of the scale of treating actual wastewater containing BDE-209 is still necessary in future research.

4. Conclusion

The degradation of BDE-209 by Fe(VI)-PMS combined process was systematically investigated in this study, which had provided an efficient method for degrading BDE-209 and controlling its toxicity. The main conclusions were summarized as follows:

The Fe(VI)-PMS combined process showed advantages in terms of effectively degrading BDE-209 and controlling toxicity, with $\bullet\text{OH}$ being confirmed as the dominant active species. The reaction kinetics were respectively 13.33 and 4.45 times higher than that in sole PMS and Fe(VI) oxidation process.

A complete removal of BDE-209 ($0.5 \mu\text{mol/L}$) was achieved within 60 min with the low dosages (0.1 mmol/L) of Fe(VI) and PMS at pH 7.0 and temperature $30 \text{ }^\circ\text{C}$, which time was reduced to 10 min by increasing the oxidants dosages to 0.5 mmol/L . In addition, over 85 % removal of BDE-209 was observed under wide range of pH (5.0–9.0), indicating the strong adaptability of Fe(VI)-PMS combined process.

BDE-209 degradation might include the reactions of debromination, radical addition, substitution, beta scission and oxidation. The detected intermediates were free bromide (66.87 %), lower brominated intermediates and even completely debrominated product.

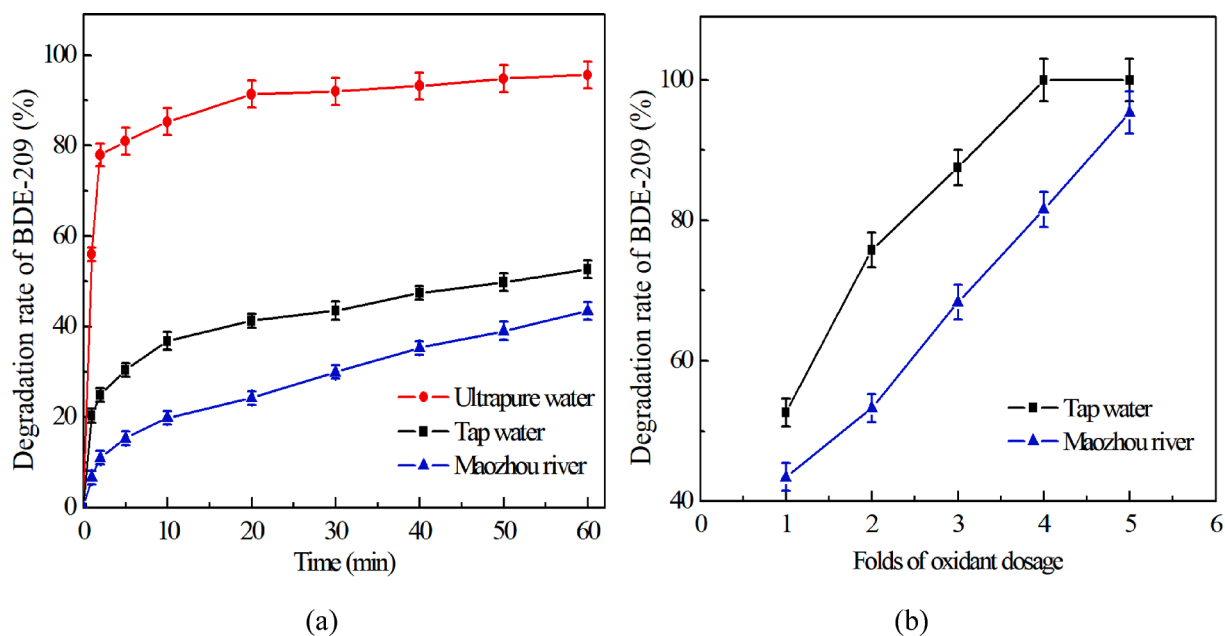


Fig. 10. (a) Degradation of BDE-209 in different water body; (b) Degradation of BDE-209 under different folds of oxidant dosages. (Experimental conditions: $C_0 = [\text{PMS}]_0 = [\text{Fe(VI)}]_0 = 0.1 \text{ mmol/L}$, $[\text{BDE-209}]_0 = 0.5 \mu\text{mol/L}$, initial solution pH = 7.0, temperature = $20 \pm 1 \text{ }^\circ\text{C}$.)

Due to the generation and accumulation of higher toxic intermediates, toxicity increased obviously at the initial stage. However, the relative inhibitory rate ($T\%=21.65\%$ at 10 min) was effectively controlled below 3.56 %, which was much lower than BDE-209 toxicity ($T\%=15.0\%$).

A 95.35 % removal rate of BDE-209 was obtained in the actual water by dosing 0.5 mmol/L oxidants, showing a prospective application of Fe(VI)-PMS combined process.

CRedit authorship contribution statement

Qi Han performed the data analyses, wrote and revised the manuscript; Yi Huang contributed to the conception of the study; Peng Liu performed the experiments; Fan Zhang and Xiaodan Chen helped perform the analysis with constructive discussions; Yurong Gu and Zijun Dong contributed to the conception of the study and contributed significantly to analysis and manuscript preparation; Boping Yu helped perform the revised the manuscript; Linshen Xie helped perform the experiments and analysis. All authors have read and agreed to the published version of the manuscript.

Declaration of competing interest

The authors declare that they have no known competing financial interests or personal relationships that could have appeared to influence the work reported in this paper.

Acknowledgements

This work was supported by the Project of Shenzhen Science and Technology Program (JCYJ20220531091403007, JCYJ20220531094416037), Shenzhen Science and Technology Innovation Committee (No. KCFXZ202002011006362) and Guangdong Basic and Applied Basic Research Foundation (No. 2021B1515120055).

Appendix A. Supplementary data

Supplementary data to this article can be found online at <https://doi.org/10.1016/j.arabjc.2024.105729>.

References

- Antoniou, M.G., Cruz, A., Dionysiou, D.D., 2010. Degradation of microcystin-LR using sulfate radicals generated through photolysis thermolysis and e-transfer mechanisms. *Appl Catal B* 96 (3–4), 290–298. <https://doi.org/10.1016/j.apcatb.2010.02.013>.
- Bruton, T.A., Sedlak, D.L., 2018. Treatment of perfluoroalkyl acids by heat-activated persulfate under conditions representative of in situ chemical oxidation. *Chemosphere* 206, 457–464. <https://doi.org/10.1016/j.chemosphere.2018.04.128>.
- Chang, Y.T., Chen, H.C., Chou, H.L., Li, H., Boyd, S.A., 2021. A coupled UV photolysis-biodegradation process for the treatment of decabrominated diphenyl ethers in an aerobic novel bioslurry reactor. *Environ. Sci. Pollut. Res.* 28, 6078–6089. <https://doi.org/10.1007/s11356-020-10753-9>.
- Chen, L., Hu, X., Yang, Y., Jiang, C., Bian, C., Liu, C., Zhang, M., Cai, T., 2018. Degradation of atrazine and structurally related triazine herbicides in soils by ferrous-activated persulfate: kinetics, mechanisms and soil-typers effects. *Chem. Eng. J.* 351 (1), 523–531. <https://doi.org/10.1016/j.cej.2018.06.045>.
- Cheng, F., He, J., Li, C., Lu, Y., Zhang, Y., Qu, J., 2021. Photo-induced degradation and toxicity change of decabromobiphenyl ethers (BDE-209) in water: effects of dissolved organic matter and halide ions. *J. Hazard. Mater.* 416 (15), 125842. <https://doi.org/10.1016/j.jhazmat.2021.125842>.
- Davies, R., Zou, E., 2012. Polybrominated diphenyl ethers disrupt molting in neonatal *Daphnia magna* [J]. *Ecotoxicology* 21 (5), 1371–1380.
- Ding, S., Wu, J., Zhang, M., Lu, H., Mahmood, Q., Zheng, P., 2015. Acute toxicity assessment of ANAMMOX substrates and antibiotics by luminescent bacteria test. *Chemosphere* 140, 174–183. <https://doi.org/10.1016/j.chemosphere.2015.03.057>.
- Dong, H., Chen, J., Feng, L., Zhang, W., Guan, X., Strathmann, T.J., 2019. Degradation of organic contaminants through activating bisulfite by Cerium(IV): a sulfate radical-predominant oxidation process. *Chem. Eng. J.* 357 (1), 328–336. <https://doi.org/10.1016/j.cej.2018.09.024>.
- Feng, M., Cizmas, L., Wang, Z., Sharma, V.K., 2017. Synergistic effect of aqueous removal of fluorquinolones by a combined use of peroxymonosulfate and ferrate(VI). *Chemosphere* 177, 144–148. <https://doi.org/10.1016/j.chemosphere.2017.03.008>.

- Giannakis, S., Lin, K.Y.A., Ghanbari, F., 2021. A review of the recent advances on the treatment of industrial wastewaters by sulfate radical-based advanced oxidation processes (SR-AOPs). *Chem. Eng. J.* 406 (15), 127083. <https://doi.org/10.1016/j.cej.2020.127083>.
- Gong, H., Chu, W., Xu, K., Xia, X., Gong, H., Tan, Y., Pu, S., 2020. Efficient degradation, mineralization and toxicity reduction of sulfamethoxazole under photo-activation of peroxymonosulfate by ferrate (VI). *Chem. Eng. J.* 389 (1), 124084. <https://doi.org/10.1016/j.cej.2020.124084>.
- Graham, N., Jiang, C.C., Li, X.Z., Jiang, J.Q., Ma, J., 2004. The influence of pH on the degradation of phenol and chlorophenols by potassium ferrate. *Chemosphere* 56 (10), 949–956. <https://doi.org/10.1016/j.chemosphere.2004.04.060>.
- Guo, S., Zhu, L., Majima, T., Lei, M., Tang, H., 2019. Reductive debromination of polybrominated diphenyl ethers: dependence on bromine number of the bromine phenyl ring. *Environ. Sci. Tech.* 53 (8), 4433–4439. <https://doi.org/10.1021/acs.est.8b07050>.
- Han W. L., Zheng X. Y., 2018. Toxicity of decabromodiphenyl ether and its degradation products to plankton [J]. *Acta Scientiae Circumstantiae*, 38(2): 821-828. 10.13671/j.hjkkxb.2017.0316.
- Han, Q., Dong, W., Wang, H., Liu, T., Sun, F., Ying, Y., Yan, X., 2013. Effects of coexisting anions on decolorization of azo dye X-3B by ferrate(VI) and a comparative study between ferrate(VI) and potassium permanganate. *Sep. Purif. Technol.* 108 (19), 74–82. <https://doi.org/10.1016/j.seppur.2013.01.053>.
- Han, Q., Wang, H., Dong, W., Liu, T., Yin, Y., Fan, H., 2015. Degradation of bisphenol a by ferrate(VI) oxidation: kinetics, products and toxicity assessment. *Chem. Eng. J.* 262 (15), 34–40. <https://doi.org/10.1016/j.cej.2014.09.071>.
- Han, Q., Dong, W., Wang, H., Liu, T., Tian, Y., Song, X., 2018. Degradation of tetrabromobisphenol a by ferrate(VI) oxidation: performance, inorganic and organic products, pathway and toxicity control. *Chemosphere* 198, 92–102. <https://doi.org/10.1016/j.chemosphere.2018.01.117>.
- Han, Q., Dong, W., Wang, H., Ma, H., Gu, Y., Tian, Y., 2019. Degradation of tetrabromobisphenol a by a ferrate(VI)-ozone combination process: advantages, optimization, and mechanistic analysis. *RSC Adv.* 9, 41783–41793. <https://doi.org/10.1039/C9RA07774J>.
- Han, Q., Wang, M., Sun, F., 2023. Effectiveness and degradation pathways of bisphenol a (BPA) initiated by hydroxyl radicals and sulfate radicals in water: initial reaction sites based on DFT prediction [J]. *Environ. Res.* 216, 114601.
- Helmy, E.T., Abouellef, E.M., Soliman, U.A., Pan, J.H., 2021. Novel green synthesis of S-doped TiO₂ nanoparticles using *Malva parviflora* plant extract and their photocatalytic, antimicrobial and antioxidant activities under sunlight illumination. *Chemosphere* 271, 129524. <https://doi.org/10.1016/j.chemosphere.2020.129524>.
- Hou, J., He, X., Zhang, S., Yu, J., Feng, M., Li, X., 2021. Recent advances in cobalt-activated sulfate radical-based advanced oxidation processes for water remediation: a review. *Sci. Total Environ.* 770 (20), 145311. <https://doi.org/10.1016/j.scitotenv.2021.145311>.
- Ji, X., Ding, J., Xie, X., Cheng, Y., Huang, Y., Qin, L., Han, C., 2017. Pollution status and human exposure of decabromodiphenyl ether (BDE-209) in China. *ACS Omega* 2 (7), 3333–3348. <https://doi.org/10.1021/acsomega.7b00559>.
- Kuo, C.Y., Pai, C.Y., Wu, C.H., Jian, M.Y., 2012. Effects of oxidant concentration and temperature on decolorization of azo dye: comparisons of UV/Fenton and UV/Fenton-like systems. *Water Sci. Technol.* 65 (11), 1970–1974. <https://doi.org/10.2166/wst.2012.095>.
- Kwon, M., Kim, S., Yoon, Y., 2015. Comparative evaluation of ibuprofen removal by UV/H₂O₂ and UV/S₂O₈²⁻ processes for wastewater treatment. *Chem. Eng. J.* 269, 379–390. <https://doi.org/10.1016/j.cej.2015.01.125>.
- Li, C., Li, X.Z., Graham, N., Gao, N.Y., 2008. The aqueous degradation of bisphenol a and steroid estrogens by ferrate. *Water Res.* 42 (1–2), 109–120. <https://doi.org/10.1016/j.watres.2007.07.023>.
- Li, C., Lin, H., Armutlulu, A., Xie, R., Zhang, Y., Meng, X., 2019. Hydroxylamine-assisted catalytic degradation of ciprofloxacin in ferrate/persulfate system. *Chem. Eng. J.* 360 (15), 612–620. <https://doi.org/10.1016/j.cej.2018.11.218>.
- Li, H.H., Zhu, F., He, S.Y., 2019. The degradation of decabromodiphenyl ether in the waste site by biochar supported nanoscale zero-valent iron /persulfate. *Ecotoxicol. Environ. Saf.* 183 (15), 109540. <https://doi.org/10.1016/j.ecoenv.2019.109540>.
- Lin, Y., Wu, S., Li, X., Wu, X., Yang, C., Zeng, G., Peng, Y., Zhou, Q., Lu, L., 2018. Microstructure and performance of Z-scheme photocatalyst of silver phosphate modified by MWCNTs and cr-doped SrTiO₃ for malachite green degradation. *Appl Catal B* 227 (5), 557–570. <https://doi.org/10.1016/j.apcatb.2018.01.054>.
- Ma, M., Chen, L., Zhao, J., Liu, W., Ji, H., 2019. Efficient activation of peroxymonosulfate by hollow cobalt hydroxide for degradation of ibuprofen and theoretical study. *Chin. Chem. Lett.* 30 (12), 2191–2195. <https://doi.org/10.1016/j.ccl.2019.09.031>.
- Ma, J., Zhang, Q., Chen, F., Lu, S., Wang, Y., Liang, H., 2021. Simultaneous removal of copper and biodegradation of BDE-209 with soil microbial cell cells. *J. Environ. Chem. Eng.* 9 (4), 105593. <https://doi.org/10.1016/j.jece.2021.105593>.
- Ma, J., Li, Y., Zhang, X., Li, J., Lin, Q., Zhu, Y., Ruan, Z., Ni, Z., Qiu, R., 2023. Modified nano zero-valent iron coupling microorganisms to degrade BDE-209: degradation pathways and microbial responses. *J. Hazard. Mater.* 465, 133378. <https://doi.org/10.1016/j.jhazmat.2023.133378>.
- Oh, W.D., Dong, Z., Lim, T.T., 2016. Generation of sulfate radical through heterogeneous catalysis for organic contaminants removal: current development, challenges and prospects. *Appl Catal B* 194 (5), 169–201. <https://doi.org/10.1016/j.apcatb.2016.04.003>.
- Panda, D., Manickam, S., 2019. Heterogeneous sono-Fenton treatment of decabromodiphenyl ether (BDE-209): debromination mechanism and transformation pathways. *Sep. Purif. Technol.* 209 (31), 914–920. <https://doi.org/10.1016/j.seppur.2018.06.069>.

- Qu, R., Li, C., Pan, X., Zeng, X., Liu, J., Huang, Q., Feng, J., Wang, Z., 2017. Solid surface-mediated photochemical transformation of decabromodiphenyl ether (BDE-209) in aqueous solution. *Water Res.* 125 (15), 114–122. <https://doi.org/10.1016/j.watres.2017.08.033>.
- Qu, S., Wang, W., Pan, X., Li, C., 2020. Improving the Fenton catalytic performance of FeOCl using an electron mediator. *J. Hazard. Mater.* 384 (15), 121494 <https://doi.org/10.1016/j.jhazmat.2019.121494>.
- Ren, Z., Romar, H., Varila, T., Xu, X., Wang, Z., Sillanpää, M., Leiviskä, T., 2021. Ibuprofen degradation using a co-doped carbon matrix derived from peat as a peroxymonosulfate activator. *Environ. Res.* 193, 110564 <https://doi.org/10.1016/j.envres.2020.110564>.
- Sarkar, D., Midha, P., Shanti, S.S., Singh, S.K., 2023. A comprehensive review on the decabromodiphenyl ether (BDE-209)-induced male reproductive toxicity: evidences from rodent studies. *Sci. Total Environ.* 901, 165938 <https://doi.org/10.1016/j.scitotenv.2023.165938>.
- Sboui, M., Al-Ghamdi, Y.O., Alamry, K.A., Hussein, M.A., Swaminathan, M., Zhao, Y., Lu, G., Ji, Z., Chen, M., Zhang, K., Pan, J.H., 2023. Multifunctional photoactive cotton fabric coated with Ag-AgI/TiO₂ nanocomposite for environmental and biological applications under sunlight [J]. *Ind. Crop Prod.* 205, 117501 <https://doi.org/10.1016/j.indcrop.2023.117501>.
- Shao, W., Zhang, W., Wang, C., Kou, Z., Yong, W., Jiao, J., Yan, W., Pang, W., 2021. BDE-209 caused gut toxicity through modulating the intestinal barrier, oxidative stress, autophagy, inflammation, and apoptosis in mice. *Sci. Total Environ.* 776 (1), 146018 <https://doi.org/10.1016/j.scitotenv.2021.146018>.
- Shi, J., Qu, R., Feng, M., Wang, X., Wang, L., Yang, S., Wang, Z., 2015. Oxidative degradation of decabromodiphenyl ether (BDE 209) by potassium permanganate: reaction pathways, kinetics, and mechanisms assisted by density functional theory calculations. *Environ. Sci. Tech.* 49 (7), 4209–4217. <https://doi.org/10.1021/es505111r>.
- Shi, M., Xia, K., Peng, Z., Jiang, Y., Dong, Y., Shi, L., 2021. Differential degradation of BDE-3 and BDE-209 by the shewanella oneidensis MR-1-mediated Fenton reaction. *Int. Biodeter. Biodegr.* 158, 105165 <https://doi.org/10.1016/j.ibiod.2020.105165>.
- Su, C., Li, R., Li, C., Wang, W., 2022. Piezo-promoted regeneration of Fe²⁺ boosts peroxydisulfate activation by Bi₂Fe₄O₉ nanosheets. *Appl Catal B* 310 (5), 121330. <https://doi.org/10.1016/j.apcatb.2022.121330>.
- Sun, S., Pang, S.Y., Jiang, J., 2018. The combination of Ferrate(VI) and sulfite as a novel advanced oxidation process for enhanced degradation of organic Contaminants[J]. *Chem. Eng. J.* 333, 11–19.
- Sun, S., Pang, S., Jiang, J., Ma, J., Huang, Z., Zhang, J., Liu, Y., Xu, C., Liu, Q., Yuan, Y., 2018. The combination of ferrate (VI) and sulfite as a novel advanced oxidation process for enhanced degradation of organic contaminants. *Chem. Eng. J.* 333 (1), 11–19. <https://doi.org/10.1016/j.cej.2017.09.082>.
- Sun, Y., Xu, Y., Wu, H., Hou, J., 2024. A critical review on BDE-209: source, distribution, influencing factors, toxicity, and degradation. *Environ. Int.* 183, 108410 <https://doi.org/10.1016/j.envint.2023.108410>.
- Tan, L., Lu, S.Y., Fang, Z.Q., et al., 2017. Enhanced reductive debromination and subsequent oxidative ring-opening of decabromodiphenyl ether by integrated catalyst of nZVI supported on magnetic Fe₃O₄ nanoparticles [J]. *Appl Catal B* 200, 200–210.
- Tiwari, J., Naoghare, P., Sivanesan, S., Bafana, A., 2017. Biodegradation and detoxification of chloronitroaromatic pollutant by cupriavidus. *Bioresour. Technol.* 223, 184–191. <https://doi.org/10.1016/j.biortech.2016.10.043>.
- Tso, C.P., Shih, Y.H., 2017. The influence of carboxymethylcellulose (CMC) on the reactivity of Fe NPs toward decabrominated diphenyl ether: the Ni doping, temperature, pH, and anion effects. *J. Hazard. Mater.* 322 (15), 145–151. <https://doi.org/10.1016/j.jhazmat.2016.03.082>.
- Wagner, W.F., Gump, J.R., Hart, E.N., 1952. Factors affecting the stability of aqueous potassium Ferrate(VI) Solutions[J]. *Anal. Chem.* 24 (9), 1497–1498.
- Wang, J., Liu, C., Wang, S.P., Zhang, T.X., Chen, J.Y., Zhou, Q., Hou, Y., Yan, Z.G., 2023. BDE-209-induced genotoxicity, intestinal damage and intestinal microbiota dysbiosis in zebrafish (danio rerio). *Sci. Total Environ.* 905, 167009 <https://doi.org/10.1016/j.scitotenv.2023.167009>.
- Wang, Z., Qiu, W., Pang, S., 2020. Relative contribution of ferryl ion species (Fe(IV)) and sulfate radical formed in nanoscale zero valent iron activated peroxydisulfate and peroxymonosulfate Processes[J]. *Water Res.* 172, 115504.
- Wu, S., Li, H., Li, X., He, H., Yang, C., 2018. Performances and mechanisms of efficient degradation of atrazine using peroxymonosulfate and ferrate as oxidants. *Chem. Eng. J.* 353 (1), 533–541. <https://doi.org/10.1016/j.cej.2018.06.133>.
- Wu, S., Lin, Y., Yang, C., Du, C., Teng, Q., Ma, Y., Zhang, D., Nie, L., Zhong, Y., 2019. Enhanced activation of peroxymonosulfate by LaFeO₃ perovskite supported on Al₂O₃ for degradation of organic pollutants. *Chemosphere* 237, 124478. <https://doi.org/10.1016/j.chemosphere.2019.124478>.
- Wu, S., Liu, H., Yang, C., Li, X., Lin, Y., Yin, K., Sun, J., Teng, Q., Du, C., Zhong, Y., 2020. High-performance porous carbon catalysts doped by iron and nitrogen for degradation of bisphenol F via peroxymonosulfate activation. *Chem. Eng. J.* 392 (15), 123683 <https://doi.org/10.1016/j.cej.2019.123683>.
- Wu, N., Qu, R., Li, C., Bin-Jumah, M., Allam, A., Cao, W., Yu, Y., Sun, C., Wang, Z., 2020. Enhanced oxidative degradation of decabromodiphenyl ether in soil by coupling Fenton-persulfate processes: insights into degradation products and reaction mechanisms. *Sci. Total Environ.* 737 (1), 139777 <https://doi.org/10.1016/j.scitotenv.2020.139777>.
- Wu, Z., Xie, M., Li, Y., Gao, G., Bartlam, M., Wang, Y., 2018. Biodegradation of decabromodiphenyl ether (BDE 209) by a newly isolated bacterium from an e-waste recycling area. *AMB Express* 8 (27), 1–12. <https://doi.org/10.1186/s13568-018-0560-0>.
- Xiong, Z., Jiang, Y., Wu, Z., Yao, G., Lai, B., 2021. Synthesis strategies and emerging mechanisms of metal-organic frameworks for sulfate radical-based advanced oxidation process: a review. *Chem. Eng. J.* 421 (1), 127863 <https://doi.org/10.1016/j.cej.2020.127863>.
- Yao, B., Luo, Z., Zhi, D., Hou, D., Luo, L., Du, S., Zhou, Y., 2021. Current progress in degradation and removal methods of polybrominated diphenyl ethers from water and soil: a review. *J. Hazard. Mater.* 403 (5), 123674 <https://doi.org/10.1016/j.jhazmat.2020.123674>.
- Yu, Y., Yin, H., Peng, H., Lu, G., Dang, Z., 2019. Biodegradation of decabromodiphenyl ether (BDE-209) using a novel microbial consortium GY1: cells viability, pathway, toxicity assessment, and microbial function prediction. *Sci. Total Environ.* 668 (10), 958–965. <https://doi.org/10.1016/j.scitotenv.2019.03.078>.
- Yu, Y., Yin, H., Huang, W., Peng, H., Lu, G., Dang, Z., 2020. Cellular changes of microbial consortium GY1 during decabromodiphenyl ether (BDE-209) biodegradation and identification of strains responsible for BDE-209 degradation in GY1. *Chemosphere* 249, 126205. <https://doi.org/10.1016/j.chemosphere.2020.126205>.
- Yunho, L., Jeyong, Y., Urs, V.G., 2005. Spectrophotometric determination of ferrate (Fe(VI)) in water by ABTS[J]. *Water Res.* 39 (10), 1946–1953. <https://doi.org/10.1016/j.watres.2005.03.005>.
- Zhang, P., Zhang, G., Dong, J., Fan, M., Zeng, G., 2012. Bisphenol a oxidative removal by ferrate (Fe(VI)) under a weak acidic condition. *Sep. Purif. Technol.* 84 (9), 46–51. <https://doi.org/10.1016/j.seppur.2011.06.022>.
- Zhao, P., Ye, Q., Zheng, Y., Whalen, K.J., Zhang, S., Wang, W., 2021. Radiolytic degradation of BDE-209 in rice-vegetable rotation soils induced by electron beam irradiation. *Environ. Pollut.* 286 (1), 117564 <https://doi.org/10.1016/j.envpol.2021.117564>.
- Zhu, Y., Chang, B., Sun, X., Luo, H., Wang, W., Li, C., 2022. Chloride-mediated electrochemical degradation of the venlafaxine antidepressant. *Environ. Technol. Innov.* 25, 102189 <https://doi.org/10.1016/j.eti.2021.102189>.